ACS Chemical Neuroscience

Letter

pubs.acs.org/chemneuro

Development of a Fluorinated Class-I HDAC Radiotracer Reveals Key Chemical Determinants of Brain Penetrance

Martin G. Strebl,[†,‡] Changning Wang,[†] Frederick A. Schroeder,[†] Michael S. Placzek,[†,§] Hsiao-Ying Wey,[†] Genevieve C. Van de Bittner,[†] Ramesh Neelamegam,[†] and Jacob M. Hooker*[,†]

[†]Athinoula A. Martinos Center for Biomedical Imaging, Massachusetts General Hospital and Harvard Medical School, 149 13th Street, Charlestown, Massachusetts 02129, United States

[‡]Department of Chemistry and Chemical Biology, Harvard University, 12 Oxford Street, Cambridge, Massachusetts 02138, United States

[§]Department of Psychiatry, McLean Imaging Center, McLean Hospital, Harvard Medical School, 115 Mill Street, Belmont, Massachusetts 02478, United States

Supporting Information

ABSTRACT: Despite major efforts, our knowledge about many brain diseases remains remarkably limited. Epigenetic dysregulation has been one of the few leads toward identifying the causes and potential treatments of psychiatric disease over the past decade. A new positron emission tomography radiotracer, [^{11}C]Martinostat, has enabled the study of histone deacetylase in living human subjects. A unique property of [^{11}C]Martinostat is its profound brain penetrance, a feature that is challenging to engineer intentionally. In order to understand determining factors for the high brain-uptake of Martinostat, a series of compounds was evaluated in rodents and nonhuman primates. The study revealed the major structural contributors to brain uptake, as well as a more clinically relevant fluorinated HDAC radiotracer with comparable behavior to Martinostat, yet longer half-life.

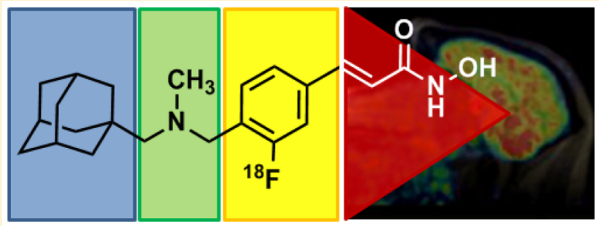

KEYWORDS: *histone deacetylase, positron emission tomography, fluorine, brain penetrance, epigenetics, blood-brain barrier*

Epigenetic dysregulation is linked to a number of diverse brain pathologies.[1−5] Histone deacetylases (HDACs) are epigenetic enzymes which have received considerable attention as potential drug targets, based on animal models and post mortem studies.[6−12] Even though their potential application includes a number of psychiatric and neurodegenerative diseases, only cancer treatment is currently an approved application of HDAC inhibitors in humans.[13] A crucial missing link toward neurological and psychiatric applications is a more detailed, quantitative understanding of HDAC enzymes and their relationship to disease and treatment inside the living human brain.

Positron emission tomography (PET) has a unique potential to visualize human epigenetic biochemistry in vivo. The rate limiting step toward understanding the human neuroepigenome with PET is the development of suitable radiotracers because a number of parameters, like brain penetrance, are still virtually impossible to determine without tedious trial-and-error based screening.[14]

[^{11}C]Martinostat is an HDAC radiotracer with exceptionally high brain uptake.[12,15,16] The currently available version of Martinostat is labeled with carbon-11, which limits its practicality, since logistics are constrained by its 20 min half-life.[17,18] One key achievement presented in this work is the development of an [^{18}F]-HDAC radiotracer, which enables in vivo quantification of HDAC with the benefits of a longer half-life. Additionally, an [^{18}F]-labeled version enabled a detailed resolution of the contribution of different functional groups to the remarkable brain uptake of Martinostat. As empirically identified, contribution of a single adamantyl substituent was confirmed[19,20] to be a major driving force for the brain penetrance of Martinostat. Furthermore, amine methylation significantly increases brain uptake.

RESULTS AND DISCUSSION

Strategic Prioritization of Candidates. To develop a fluorine-18 analogue of [^{11}C]Martinostat, we attempted two distinct strategies: (1) labeling by installation of a fluorine-bearing prosthetic group or (2) fluorination of the aromatic ring. The first approach is represented by CN146, which contains a fluoroethyl substituent, while the second approach is actualized by the structures MGS1−3, which are labeled on the aromatic ring (Figure 1). Ex vivo prioritization of compounds was achieved using a validated functional recombinant HDAC assay to determine the extent to which candidate structures engage HDAC subtypes.[15] As shown in Figure 1, installation of

Received: November 10, 2015
Accepted: December 16, 2015
Published: December 16, 2015

DOI: 10.1021/acschemneuro.5b00297
ACS Chem. Neurosci. 2016, 7, 528−533

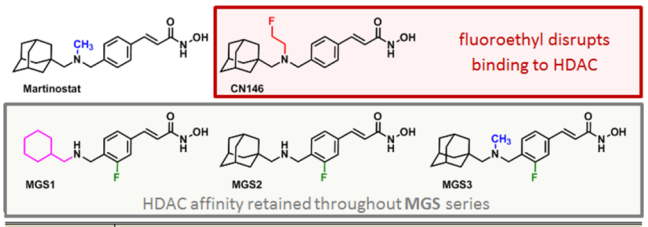

IC50 (nM)	HDAC1	HDAC2	HDAC3	HDAC6	HDAC8
Martinostat	0.3	0.8	0.6	4.1	>15000
CN146	222	651	470	308	>30000
MGS1	1.64	14.2	0.54	11.7	725
MGS2	0.8	6.4	0.5	9.5	>5000
MGS3	0.78	7.0	0.76	11.6	>30000

Figure 1. Recombinant HDAC assay and IC_{50} values for candidate molecules to elucidate how structural modifications to [^{12}C]-Martinostat impact target engagement. While installation of a fluoroethyl prosthetic group disrupts HDAC binding, the target affinity is retained throughout the MGS series.

a fluoroethyl prosthetic group reduces HDAC affinity drastically. Therefore, we focused our efforts on three leads, MGS1–3.

Initial interrogation of brain uptake of the MGS1–3 series utilizing the existing [^{11}C]Martinostat radiotracer indicated a comparable reduction in [^{11}C]Martinostat uptake in rat following administration of either 1 mg/kg of unlabeled [^{19}F]MGS1–3 or unlabeled [^{12}C]Martinostat (Figure 1-SI), providing evidence for brain penetrance and in vivo HDAC engagement of the candidate structures and warranting investments in radiolabeling.

Rodent PET-CT. To verify in vivo specific, saturable binding of the three candidate structures, MGS1–3, to HDAC, we radiolabeled each compound with fluorine-18. Although yields were generally low (Supporting Information), we obtained sufficient amounts in high specific activity to conduct dynamic PET/CT imaging in rodents. The time–activity curves (TACs) of a whole-brain volume of interest (VOI) at baseline were compared to intravenous pretreatment with 1 mg/kg of unlabeled [^{12}C]Martinostat immediately prior to radiotracer injection.[12] As shown in Figure 2, all fluorine-18 tracers showed similar baseline TAC profiles, including a rapid increase in whole brain activity with peak activity around 10 min post injection, and limited washout over the 2 h scan interval. Consistent with saturable in vivo binding, pretreatment with a brain-penetrant HDAC inhibitor increases the rate of [^{18}F]MGS1–3 washout, resulting in a 40–50% reduction in [^{18}F]MGS1–3 compared to peak activity within 2 h (Figure 2). This observation indicates in vivo HDAC engagement of MGS1–3 signal in rodents is predominantly due to saturable, and hence specific binding to their respective targets.

Nonhuman Primate Imaging. To determine the degree to which specific structural changes of tracer molecules impact brain penetrance and in vivo distribution, as well as for validation of the compounds in a higher species, we advanced MGS1–3 to nonhuman primates. Dynamic PET/MRI imaging in baboon (*Papio anubis*) revealed differences between the labeled molecules in greater detail. Brain images of [^{18}F]MGS1–3 standardized uptake value (SUV), summed over 30–60 min postradiotracer injection, are shown in comparison to [^{11}C]Martinostat in Figure 3. All three tracers penetrate the blood brain barrier, but the overall SUV greatly varies across the substitution patterns, indicated by the gray bar next to the images. While MGS3 reaches about 78% of the uptake of [^{11}C]Martinostat, seemingly minor structural changes have a detrimental influence on the uptake properties. Formal removal of the methyl group on the amine, as shown by MGS2, results in only about 52% of the uptake of [^{11}C]Martinostat, which is equivalent to an additional 33% reduction of brain uptake with compared to MGS3. Even more strikingly, substitution of the adamantyl substituent for cyclohexyl results in an SUV of 0.56, a 69% decrease compared to MGS3.

Brain penetrance often correlates to specific physical properties of molecules within a series (Table 1), such as their distribution coefficient (LogP) or total polar surface area (TPSA).[21] In the case of [^{18}F]MGS1–3, it is true that, with a higher computed LogP (cLogP),[22,23] brain penetrance increases. The cLogP of MGS1–3 (3.07, 3.77, 4.17, respectively) correlate linearly (R^2 = 0.99) with the SUV. In

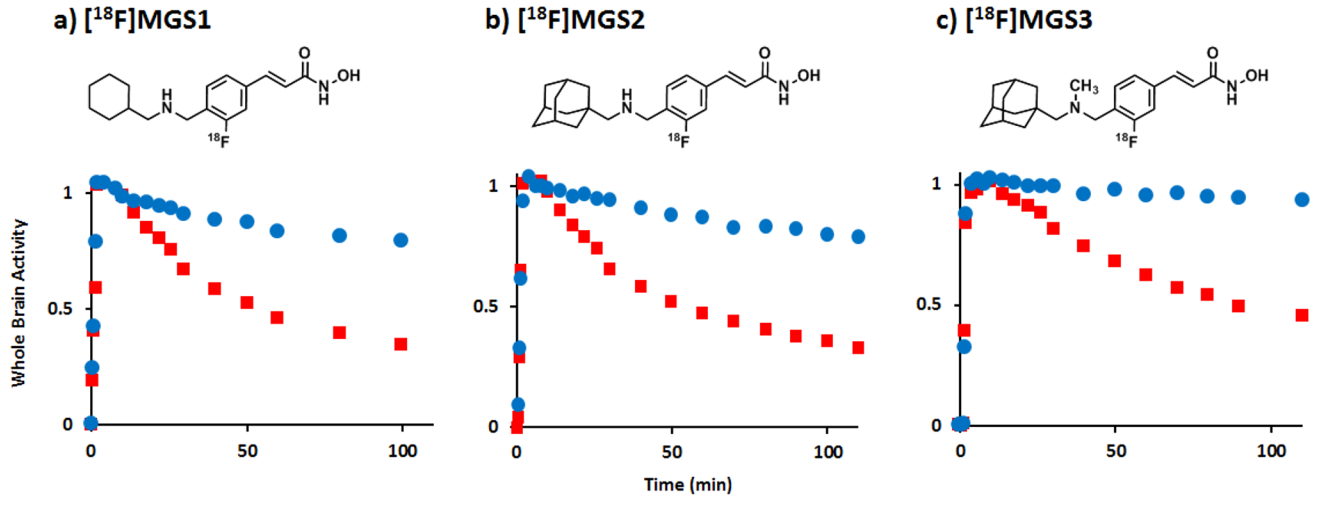

Figure 2. PET-CT Imaging of [^{18}F]MGS1–3 in rat. Graphs show tracer uptake in brain at baseline and after pretreatment with [^{12}C]Martinostat (1 mg/kg), normalized to whole brain activity at 10 min post injection. Robust blocking was observed for all three tracers: (a) [^{18}F]MGS1, (b) [^{18}F]MGS2, and (c) [^{18}F]MGS3. Time–activity curves for whole brain VOI (baseline, blue; blocking, red) confirm high specific/nonspecific binding ratio for all three molecules, as the retained activity after 2 h is markedly reduced by administration of a blocking agent.

DOI: 10.1021/acschemneuro.5b00297
ACS Chem. Neurosci. 2016, 7, 528–533

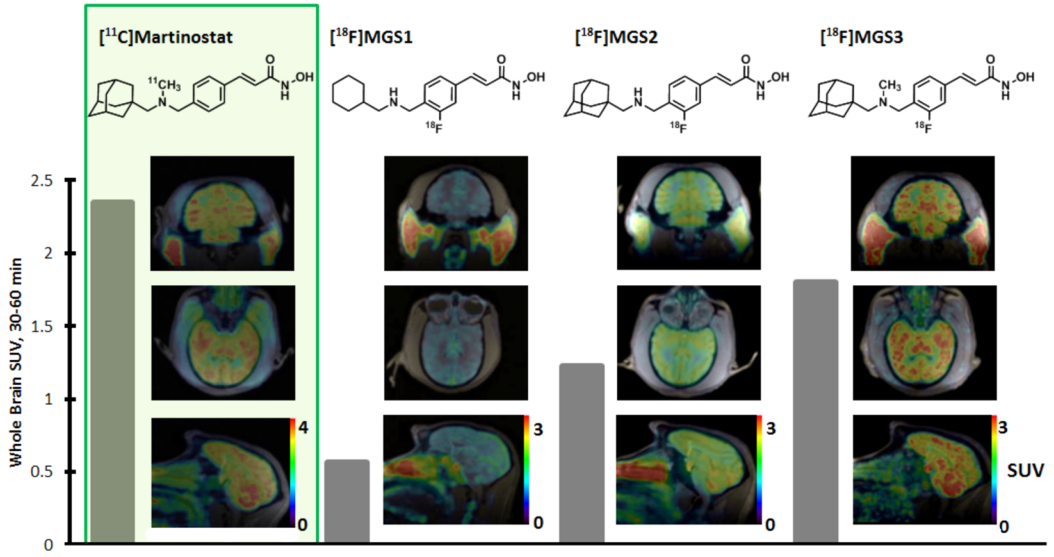

Figure 3. Whole brain radiotracer uptake. Images show the distribution of [^{11}C]Martinostat (SUV scale 0−4) as well as [^{18}F]MGS1−3 (SUV scale 0−3) in baboon brain in three planes each. The images are shown in subject space. The respective whole brain SUVs (30−60 min) are quantified for each tracer by the gray bar.

Table 1. Physical Properties and Standardized Uptake Values of the MGS Series

Radiotracer	[^{18}F] MGS1	[^{18}F]MGS2	[^{18}F]MGS3
SUV, baboon	0.566	1.22	1.80
cLogP	3.07	3.77	4.17
TPSA	61.35	61.35	52.56

comparison, the TPSA values of 61.35 for both MGS1 and 2, and 52.56 for [^{18}F]MGS3 do not seem to correlate well with the observed behavior. It has previously been suggested that the high brain penetrance of adamantyl bearing structures can be explained by an increased lipophilicity, with a rigid and constricted atomic configuration compared to linear alkanes, which typically leads to undesirable nonspecific binding.[20] Our findings are consistent with that hypothesis.

Apart from the adamantyl substituent, another factor we were specifically interested in was the influence of amine methylation on brain uptake, which was tested through comparison of MGS2 and MGS3. Formal removal of a methyl group from the parent structure is estimated to decrease the pK_a by roughly one unit. However, at physiological pH, this change is not expected to alter the protonation state significantly, since pK_a values of secondary and tertiary acyclic aliphatic amines are typically greater than 9.[24] The influence on the cLogP and, ultimately, the SUV is nonetheless profound, as described above. The effect of methylation on brain uptake within the MGS-series is therefore merely based on overall polarity.

Beyond brain uptake, the regional tracer distribution was assessed to determine the suitability of a candidate fluorine-18 tracer as an analogue for [^{11}C]Martinostat. To compare regional distribution, images for each tracer were coregistered to the Black baboon atlas,[25] 38 ROIs were chosen, and symmetrical regions averaged. The regional SUV values for [^{18}F]MGS1−3 were determined and compared to [^{11}C]-Martinostat (Figure 4, Table 1-SI). While for [^{18}F]MGS1, the correlation is relatively poor (but still significant, Spearman r = 0.64, P = 0.005), correlation increases across the series to [^{18}F]MGS3 (Spearman r = 0.86, $P = 3.5 \times 10^{-6}$). This degree of correlation strongly suggests a high specific binding

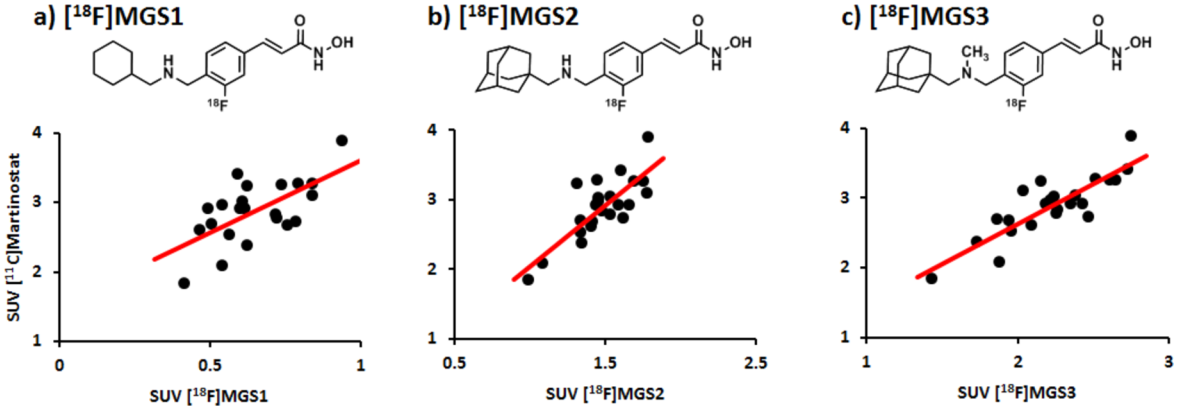

Figure 4. Regional correlation between [^{11}C]Martinostat and the MGS series. (a) Regional correlation analysis between [^{11}C]Martinostat and [^{18}F]MGS1 averaged 30−60 min after TOI, Spearman r = 0.64; (b) [^{11}C]Martinostat and [^{18}F]MGS2 averaged 30−60 min after TOI, Spearman r = 0.79; and (c) [^{11}C]Martinostat and [^{18}F]MGS3 averaged 30−60 min post injection, Spearman r = 0.86;.

DOI: 10.1021/acschemneuro.5b00297
ACS Chem. Neurosci. 2016, 7, 528−533

component as well as engagement of the same targets as [^{11}C]Martinostat.

The results presented here are limited by several consequences of the inefficient radiochemistry. Poor yields and the manual synthesis only allowed for low doses to be administered. Full validation of [^{18}F]MGS3, including blocking experiments in baboons, rigorous kinetic quantification using an arterial input function, and automated production for human use will require a more efficient synthesis, which is currently under investigation. Our laboratory is investigating the detailed contributions of HDAC subtypes in different tissues to the overall signal.

CONCLUSION

We developed a series of new fluorine-18 labeled radiotracers for measuring HDAC occupancy in the central nervous system. It was found that, within the examined series, the major driving force for brain uptake could be attributed to an adamantyl substituent. Additionally, it was determined that methylation of an amine moiety also drastically increases SUV, overall affording the desired replacement for [^{11}C]Martinostat. [^{18}F]MGS3 exhibits specific binding, as well as comparable brain uptake and regional distribution to [^{11}C]Martinostat, which warrants further investigation of more efficient radiosyntheses to facilitate full imaging validation and enable use in human subjects.

METHODS

Animal Preparation. *Rodent.* A total of 12 male Sprague−Dawley rats (Charles River Laboratories) between 2 and 4 months of age were used for imaging. Animals were pair-housed until they reached a weight of 500 g, and were kept on a 12 h/12 h light/dark cycle. All treatment and imaging experiments were performed according to procedures approved by the Institutional Animal Care and Use Committee at the Massachusetts General Hospital. Anesthesia consisting of isoflurane (3% for induction, 2% for maintenance) and oxygen carrier was administered to each animal. For i.v. administration, a catheter was placed in a lateral tail vein of each animal. The catheter was connected to a syringe via an extension line. Animals received a bolus injection of either vehicle (1:1:8 DMSO/Tween80/saline) or blocking agent in solution (1 mg/kg, 1 mg/mL in 1:1:8 DMSO/Tween80/saline) immediately prior to injection of the radiotracer.

NHP. Four baseline PET/MR studies were carried out with two baboons (both females, *Papio anubis*, 13.4 and 16.2 kg) as approved by the Institutional Animal Care and Use Committee at the Massachusetts General Hospital. Nil per os was instructed 12 h prior to the study. Anesthesia was induced with intramuscular (i.m.) ketamine (10 mg/kg) and xylazine (0.5 mg/kg). Anesthesia was continued during the study with 1−1.5% isoflurane in medical oxygen, and ketamine/xylazine effects were reverted with yobine (0.11 mg/kg, i.m.) prior to the scan. Radiotracer injection was performed through a catheter in the saphenous vein. Vital signs (end-tidal CO_2, oxygen saturation, heart rate, and respiration rate) were under continuous surveillance to maintain a normal physiological range, documented every 15 min.

Chemical Synthesis. Syntheses and characterization of blocking agents, precursors for radiolabeling, reagents, and nonradioactive standards are described in detail in the Supporting Information.

Radiosynthesis. [^{11}C]Martinostat was synthesized as previously reported.[6,7] Radiosyntheses for MGS1−3 are described in detail in the Supporting Information.

PET/MR Image Acquisition. *Rodent.* After injection of a radiotracer bolus (669 ± 15 μCi [^{11}C]Martinostat; 305 ± 5 μCi [^{18}F]MGS1; 103 ± 4 μCi [^{18}F]MGS2; 67 ± 1 μCi [^{18}F]MGS3), a 120 min dynamic PET scan was acquired for each animal. PET scans were performed on either a GammaMedica Triumph PET/CT/SPECT scanner or Siemens P4 PET scanner. PET data collected on the GammaMedica Triumph was corrected for attenuation with the corresponding CT image, which was acquired immediately following the PET scan. On the P4 scanner, a transmission scan with a Cobalt (^{57}Co) line source was acquired to generate an attenuation map, which was applied during image reconstruction. The dynamic PET data was binned into 38 *or* 44 timeframes (8 × 15 s, 8 × 1 min, 10 × 2 min, 18 × 5 min *or* 6 × 5 min and 6 × 10 min) and reconstruction of each frame via an iterative MLEM (maximum likelihood expectation maximization) algorithm, consisting of 16 iterations, afforded images with a resolution of approximately 2 mm fwhm (full width at half-maximum).

NHP. PET/MRI acquisition was performed on a 3T Siemens TIM-Trio with a BrainPET insert (Siemens, Erlangen, Germany). A PET/MRI compatible eight-channel array coil customized for nonhuman primate brain imaging to increase image signal and quality was employed. After administration of one of the radiotracers (1.4 mCi MGS1; 1.8 mCi MGS2; 0.55 mCi MGS3) or [^{11}C]Martinostat (4.9 mCi), dynamic PET image acquisition was initiated. Dynamic PET data were collected and stored in list mode for 90 min in the case of [^{11}C]Martinostat and 120 min for [^{18}F]MGS1−3. Image reconstruction was performed using the 3D ordinary Poisson expectation maximization algorithm with detector efficiency, decay, dead time, attenuation, and scatter corrections. PET data were binned in 29 frames (6 × 10 s, 6 × 20 s, 2 × 30 s, 1 × 1 min, 5 × 5 min, 9 × 10 min for [^{18}F] scans (6 × 10 min for [^{11}C]Martinostat)). Image volumes were eventually reconstructed into 76 slices with 128 × 128 pixels and a 2.5 mm isotropic voxel size. Thirty minutes after scanner start, a high-resolution anatomical scan using multiecho MPRAGE sequence (TR = 2530 ms, TE1/TE2/TE3/TE4 = 1.64/3.5/5.36/7.22 ms, TI = 1200 ms, flip angle = 7°, and 1 mm isotropic) was acquired.

Image Analysis. *Rodent.* The imaging software package PMOD 3.3 (PMOD Technologies, Zurich, Switzerland) was used for all image analysis. All PET imaging data acquired on the Triumph scanner were coregistered to the CT image acquired from the same animal. Siemens P4 data were aligned and coregistered to CT data derived from an age matched animal of similar size. For maximum consistency, the data were coregistered to the Schiffer Px Rat[26] rat brain template and data was derived from a whole brain VOI (volumes of interest) for time activity curves.

NHP. PET data were registered to the Black baboon brain atlas[25] using JIP tools optimized for nonhuman primate data processing (www.nitrc.org/projects/jip). The high-resolution T1-weighted anatomical MRI image was first registered to the baboon brain atlas using a mutual information approach and the transformation parameters were then applied to the simultaneously collected dynamic PET data. Thirty-eight common VOIs from the Black baboon atlas[25] were applied to all scans. Time−activity curves (TACs) were extracted from the orbitofrontal cortex, dorsolateral prefontal cortex, anterior cingulate gyrus, posterior cingulate gyrus, amygdala, hippocampus, ventral caudate, caudate body, putamen, nucleus accumbens, medial and ventral posterolateral thalamus, habenula, cerebellar midline nuclei, whole cerebellum, genu and splenium of the corpus callosum, striate cortex, motor cortex, supplementary motor area, and the centrum semiovale. Symmetrical structures were averaged before further analysis. For SUV calculations, time points between 30 and 60 min were averaged for each tracer and each VOI. Spearman correlation coefficients, R^2 values, and P values were determined using statistical tools within Microsoft Excel.

ASSOCIATED CONTENT

Supporting Information

The Supporting Information is available free of charge on the ACS Publications website at DOI: 10.1021/acschemneuro.5b00297.

HDAC inhibition assay, chemical syntheses, radiosyntheses of MGS1−3, blocking experiments with nonlabeled MGS1−3 and detailed regional analysis of

DOI: 10.1021/acschemneuro.5b00297
ACS Chem. Neurosci. 2016, 7, 528−533

brain distribution of MGS3 in comparison to Martinostat (PDF)

AUTHOR INFORMATION

Corresponding Author

*E-mail: hooker@nmr.mgh.harvard.edu.

Author Contributions

M.G.S. developed radiosyntheses of all [^{18}F]MGS tracers, synthesized them for rodent and nonhuman primate experiments, assisted in the design of imaging experiments, carried out PET image analysis and synthesized nonradioactive blocking compounds. C.W. synthesized [^{11}C]Martinostat for imaging experiments, synthesized nonradioactive blocking compounds, assisted in the design of imaging experiments and coordinated IC_{50} measurements. F.A.S. designed and assisted with blocking experiments and assisted with rodent image analysis for blocking experiments. M.S.P. assisted with rodent PET scans and carried out image analysis of [^{18}F]MGS1-3. H.-Y.W. coordinated and assisted in nonhuman primate imaging, carried out nonhuman primate image coregistration to atlas space and assisted with image analysis. G.C.V.d.B. assisted with design and execution of rodent imaging. R.N. assisted with the synthesis of nonradioactive inhibitors and preliminary radiosynthesis. J.M.H. conceived and supervised the project. The manuscript was written through contributions of all the authors. All authors have given approval to the final version of the manuscript.

Funding

M.G.S. was supported by a training grant from the NIH Blueprint for Neuroscience Research (T90DA022759/R90DA023427), as well as the Jacques-Emile Dubois Graduate Student Dissertation Fellowship Fund. C.W. and H.-Y.W. were supported by the Harvard/MGH Nuclear Medicine Training Program from the Department of Energy (DE-SC0008430). M.S.P. was supported by a NIH-NIDA T32 postdoctoral fellowship (T32DA015036). H.-Y.W. is supported by a NIDA K99/R00 grant (K99DA037928). G.C.V.d.B. was supported by the Nuclear Med Training grant (DE-SC0008430). Research was supported by the National Institute of Drug Abuse (NIDA) of the National Institutes of Health under Grant Number R01DA030321. This research was carried out at the Athinoula A. Martinos Center for Biomedical Imaging at the Massachusetts General Hospital, using resources provided by the Center for Functional Neuroimaging Technologies, P41EB015896, a P41 Regional Resource supported by the National Institute of Biomedical Imaging and Bioengineering (NIBIB), National Institutes of Health. This work also involved the use of instrumentation supported by the NIH Shared Instrumentation Grant Program and/or High-End Instrumentation Grant Program; specifically, Grant Numbers S10RR017208, S10RR026666, S10RR022976, S10RR019933, and S10RR029495.

Notes

The authors declare no competing financial interest.

ACKNOWLEDGMENTS

The authors are grateful to Helen Deng as well as the Martinos Center radiopharmacy and imaging staff (Grae Arabasz, Regan Butterfield, Garima Gautam, Shirley Hsu, Kari Phan, Judit Sore, and Samantha To) for help with nonhuman primate experiments and isotope generation. HDAC activity screening was enabled by a Caliper assay developed by Jennifer Gale and Yan-Ling Zhang at the Broad Institute. Thanks to Tonya Gilbert for helpful discussions.

REFERENCES

(1) Akbarian, S., and Nestler, E. J. (2013) Epigenetic Mechanisms in Psychiatry. *Neuropsychopharmacology 38*, 1−2.

(2) Fass, D. M., Reis, S. A., Ghosh, B., Hennig, K. M., Joseph, N. F., Zhao, W.-N., Nieland, T. J. F., Guan, J.-S., Groves Kuhnle, C. E., Tang, W., Barker, D. D., Mazitschek, R., Schreiber, S. L., Tsai, L.-H., and Haggarty, S. J. (2013) Crebinostat: A novel cognitive enhancer that inhibits histone deacetylase activity and modulates chromatin-mediated neuroplasticity. *Neuropharmacology 64*, 81−96.

(3) Grayson, D. R., and Guidotti, A. (2013) The Dynamics of DNA Methylation in Schizophrenia and Related Psychiatric Disorders. *Neuropsychopharmacology 38*, 138−166.

(4) Robison, A. J., and Nestler, E. J. (2011) Transcriptional and epigenetic mechanisms of addiction. *Nat. Rev. Neurosci. 12*, 623−637.

(5) Sun, H., Kennedy, P. J., and Nestler, E. J. (2013) Epigenetics of the Depressed Brain: Role of Histone Acetylation and Methylation. *Neuropsychopharmacology 38*, 124−137.

(6) Schroeder, F. A., Lewis, M. C., Fass, D. M., Wagner, F. F., Zhang, Y.-L., Hennig, K. M., Gale, J., Zhao, W.-N., Reis, S., Barker, D. D., Berry-Scott, E., Kim, S. W., Clore, E. L., Hooker, J. M., Holson, E. B., Haggarty, S. J., and Petryshen, T. L. (2013) A Selective HDAC 1/2 Inhibitor Modulates Chromatin and Gene Expression in Brain and Alters Mouse Behavior in Two Mood-Related Tests. *PLoS One 8*, e71323.

(7) Jakovcevski, M., Bharadwaj, R., Straubhaar, J., Gao, G., Gavin, D. P., Jakovcevski, I., Mitchell, A. C., and Akbarian, S. (2013) Prefrontal Cortical Dysfunction After Overexpression of Histone Deacetylase 1. *Biol. Psychiatry 74*, 696−705.

(8) Bahari-Javan, S., Maddalena, A., Kerimoglu, C., Wittnam, J., Held, T., Bähr, M., Burkhardt, S., Delalle, I., Kügler, S., Fischer, A., and Sananbenesi, F. (2012) HDAC1 Regulates Fear Extinction in Mice. *J. Neurosci. 32*, 5062−5073.

(9) Guan, J.-S., Haggarty, S. J., Giacometti, E., Dannenberg, J.-H., Joseph, N., Gao, J., Nieland, T. J. F., Zhou, Y., Wang, X., Mazitschek, R., Bradner, J. E., DePinho, R. A., Jaenisch, R., and Tsai, L.-H. (2009) HDAC2 negatively regulates memory formation and synaptic plasticity. *Nature 459*, 55−60.

(10) Malvaez, M., McQuown, S. C., Rogge, G. A., Astarabadi, M., Jacques, V., Carreiro, S., Rusche, J. R., and Wood, M. A. (2013) HDAC3-selective inhibitor enhances extinction of cocaine-seeking behavior in a persistent manner. *Proc. Natl. Acad. Sci. U. S. A. 110*, 2647−2652.

(11) Kennedy, P. J., Feng, J., Robison, A. J., Maze, I., Badimon, A., Mouzon, E., Chaudhury, D., Damez-Werno, D. M., Haggarty, S. J., Han, M. H., Bassel-Duby, R., Olson, E. N., and Nestler, E. J. (2013) Class I HDAC inhibition blocks cocaine-induced plasticity by targeted changes in histone methylation. *Nat. Neurosci. 16*, 434−440.

(12) Schroeder, F. A., Wang, C., Van de Bittner, G. C., Neelamegam, R., Takakura, W. R., Karunakaran, A., Wey, H. Y., Reis, S. A., Gale, J., Zhang, Y. L., Holson, E. B., Haggarty, S. J., and Hooker, J. M. (2014) PET imaging demonstrates histone deacetylase target engagement and clarifies brain penetrance of known and novel small molecule inhibitors in rat. *ACS Chem. Neurosci. 5*, 1055−1062.

(13) West, A. C., and Johnstone, R. W. (2014) New and emerging HDAC inhibitors for cancer treatment. *J. Clin. Invest. 124*, 30−39.

(14) Van de Bittner, G. C., Ricq, E. L., and Hooker, J. M. (2014) A Philosophy for CNS Radiotracer Design. *Acc. Chem. Res. 47*, 3127−3134.

(15) Wang, C., Schroeder, F. A., Wey, H.-Y., Borra, R., Wagner, F. F., Reis, S., Kim, S. W., Holson, E. B., Haggarty, S. J., and Hooker, J. M. (2014) In Vivo Imaging of Histone Deacetylases (HDACs) in the Central Nervous System and Major Peripheral Organs. *J. Med. Chem. 57*, 7999−8009.

(16) Wey, H.-Y., Wang, C., Schroeder, F. A., Logan, J., Price, J. C., and Hooker, J. M. (2015) Kinetic Analysis and Quantification of

DOI: 10.1021/acschemneuro.5b00297
ACS Chem. Neurosci. 2016, 7, 528−533

[^{11}C]Martinostat for in Vivo HDAC Imaging of the Brain. *ACS Chem. Neurosci. 6*, 708−715.
(17) Ren, H., Wey, H.-Y., Strebl, M., Neelamegam, R., Ritter, T., and Hooker, J. M. (2014) Synthesis and Imaging Validation of [^{18}F]-MDL100907 Enabled by Ni-Mediated Fluorination. *ACS Chem. Neurosci. 5*, 611−615.
(18) Wooten, D. W., Moraino, J. D., Hillmer, A. T., Engle, J. W., Dejesus, O. J., Murali, D., Barnhart, T. E., Nickles, R. J., Davidson, R. J., Schneider, M. L., Mukherjee, J., and Christian, B. T. (2011) In vivo kinetics of [F-18]MEFWAY: a comparison with [C-11]WAY100635 and [F-18]MPPF in the nonhuman primate. *Synapse 65*, 592−600.
(19) Tsuzuki, N., Hama, T., Kawada, M., Hasui, A., Konishi, R., Shiwa, S., Ochi, Y., Futaki, S., and Kitagawa, K. (1994) Adamantane as a brain-directed drug carrier for poorly absorbed drug. 2. AZT derivatives conjugated with the 1-adamantane moiety. *J. Pharm. Sci. 83*, 481−484.
(20) Liu, J., Obando, D., Liao, V., Lifa, T., and Codd, R. (2011) The many faces of the adamantyl group in drug design. *Eur. J. Med. Chem. 46*, 1949−1963.
(21) Molinspiration Property Calculation Services, www.molinspiration.com, 2002.
(22) Tetko, I. V., Gasteiger, J., Todeschini, R., Mauri, A., Livingstone, D., Ertl, P., Palyulin, V. A., Radchenko, E. V., Zefirov, N. S., Makarenko, A. S., Tanchuk, V. Y., and Prokopenko, V. V. (2005) Virtual computational chemistry laboratory–design and description. *J. Comput.-Aided Mol. Des. 19*, 453−463.
(23) VCCLAB, Virtual Computational Chemistry Laboratory, www.vcclab.org, 2005.
(24) Bordwell, F. G. (1988) Equilibrium acidities in dimethyl sulfoxide solution. *Acc. Chem. Res. 21*, 456−463.
(25) Black, K. J., Snyder, A. Z., Koller, J. M., Gado, M. H., and Perlmutter, J. S. (2001) Template images for nonhuman primate neuroimaging: 1. Baboon. *NeuroImage 14*, 736−743.
(26) Schiffer, W. K., Mirrione, M. M., Biegon, A., Alexoff, D. L., Patel, V., and Dewey, S. L. (2006) Serial microPET measures of the metabolic reaction to a microdialysis probe implant. *J. Neurosci. Methods 155*, 272−284.

DOI: 10.1021/acschemneuro.5b00297
ACS Chem. Neurosci. 2016, 7, 528−533